Thermal radiation of laser heated niobium clusters Nb N + , 8 N 22

Klavs Hansen, Yejun Li, Vladimir Kaydashev, and Ewald Janssens

Citation: The Journal of Chemical Physics **141**, 024302 (2014); doi: 10.1063/1.4885364
View online: http://dx.doi.org/10.1063/1.4885364
View Table of Contents: http://scitation.aip.org/content/aip/journal/jcp/141/2?ver=pdfcov
Published by the AIP Publishing

Thermal radiation of laser heated niobium clusters Nb_N^+, $8 \leq N \leq 22$

Klavs Hansen,[1] Yejun Li,[2] Vladimir Kaydashev,[2] and Ewald Janssens[2]
[1]*Department of Physics, University of Gothenburg, 41296 Gothenburg, Sweden*
[2]*Laboratory of Solid State Physics and Magnetism, KU Leuven, B-3001 Leuven, Belgium*

(Received 18 April 2014; accepted 16 June 2014; published online 8 July 2014)

The thermal radiation from small, laser heated, positively charged niobium clusters has been measured. The emitted power was determined by the quenching effect on the metastable decay, employing two different experimental protocols. The radiative power decreases slightly with cluster size and shows no strong size-to-size variations. The magnitude is 40–50 keV/s at the timescale of several microseconds, which is the measured crossover time from evaporative to radiative cooling. © *2014 AIP Publishing LLC*. [http://dx.doi.org/10.1063/1.4885364]

I. INTRODUCTION

Thermal radiation and thermionic emission have been established as important decay channels for highly excited clusters of refractory materials.[1–9] Both thermal electron and photon emission are of potential technological interest, in connection with electron emitting devices or incandescent light sources.[10] In addition to possible applications, it is also of fundamental interest to study the competition between the different decay mechanisms of highly excited clusters. In most materials, the activation energy for evaporation of a massive fragment (atom or molecule) is lower than the ionization energy. This in combination with the higher frequency factor, occasionally very much higher,[11] for atomic or molecular evaporation compared with the electron emission channel, strongly favors unimolecular fragmentation reactions. For refractory materials, the high binding energy makes the thermionic emission channel competitive, and also thermal radiation, i.e., thermal emission of photons, appears on the timescales ($\sim$100 μs) defined by molecular beam devices.[12] This happens because the higher activation energies can sustain higher internal energies per atom, corresponding to higher effective temperatures, which will increase the emitted radiative power. The power may vary as the Stefan-Boltzmann T^4 law but can be modified by the finite size of the particles and the presence of resonances. This happens for the well-studied case of fullerenes where the power on the temperature dependence changes from T^4 to T^6 due to the large oscillator strength surface plasmon resonance.[13] Another important feature of thermal radiation is the absence of an activation energy. Radiation is only suppressed relative to atomic evaporation due to the larger frequency factor of the latter. This changes at low excitation energy where a crossover from atomic evaporation or thermionic emission to thermal radiation occurs.[14]

A number of bulk transition metals (Nb, W, Mo, etc.) are known as good thermal radiation emitters. Atomic clusters of these transition metals are good candidates to investigate the competing channels of atom evaporation, thermionic emission, and thermal radiation following optical excitation. Clusters of niobium are one of the species known to emit atoms,[3,15] electrons,[3,16] and photons[14,17] in thermal processes on the nano- and microsecond timescales. Several experimental studies on large but non-size-selected clusters have reported on the black-body radiation spectra of laser-heated clusters[14,18] and of clusters heated by oxidation.[17] Determining the competition between evaporation and radiation from these experiments requires modeling with more or less known input parameters.[19]

A more direct way of determining the thermal radiation is available and has been used in the experiments presented here, viz., measuring the quenching effect of radiation on the unimolecular decay. This method has not yet, to the best of our knowledge, been used to investigate refractory metal clusters. Although the method is not free of assumptions, it is based on the well tested systematics associated with the evaporative ensemble. Basically it consists of measuring the reduction of metastable decay relative to the hypothetical situation with non-radiative decay.[12]

In the remainder of the article, the experimental procedure and results will be described, together with the most important features specific to this experiment, followed by a derivation of the equations relevant for the analysis, including an evaluation of several of the approximations made. Next, the analysis is applied to the measured data, Nb_N^+ with $8 \leq N \leq 22$. A discussion of the results follows, including the consequences for the interpretation of other experiments involving evaporation and thermionic emission. Finally, the results are summarized.

II. EXPERIMENTAL PROCEDURE AND RESULTS

The clusters were produced in a laser vaporization source,[20] operated with a pulsed Nd:YAG laser (532 nm, 10 Hz) with pulse energies of about 50 mJ. He gas at a backing pressure of 8 bar was introduced by a pulsed supersonic valve into a waiting room chamber just before laser ablation of the Nb target, which was of 99.98% purity. The clusters were thermalized by heat exchange via the He carrier gas to the chamber and nozzle that were both held at room temperature. The central part of the cluster beam was selected by a conical skimmer and entered the extraction region where cationic clusters were accelerated into a reflectron

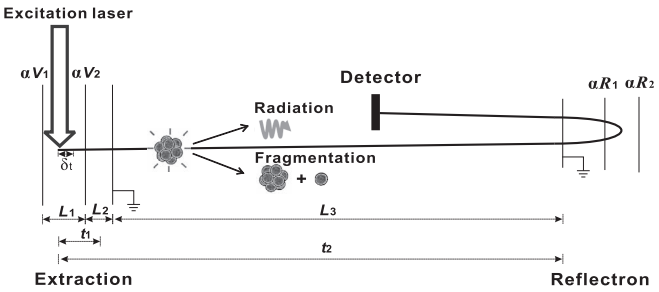

FIG. 1. A schematic drawing of the experimental setup. The lengths are $L_1 = 21$ mm, $L_2 = 10$ mm, and $L_3 = 1206$ mm. The voltages $V_1 = 3540$ V, $V_2 = 2960$ V, $R_1 = 2224$ V, and $R_2 = 3680$ V are the voltages applied on the extraction and reflectron plates at scaling factor $\alpha = 1$ (see main text for the meaning of α). The times δt, t_1, and t_2, indicated as distances, are explained in the main text below.

time-of-flight mass spectrometer (TOF). A schematic drawing of the setup is shown in Fig. 1 where also the most important dimensions are given.

The extraction stage of the TOF consists of a dual field region. The ionization and excitation was performed in the first acceleration stage with a second harmonic pulse of a Nd:YAG laser (532 nm, 10 Hz, 15 ns). The laser beam diameter (0.5 cm) was optimized to have maximal spatial overlap with the cluster beam. The energy used for photo-fragmentation was monitored with a pyroelectric energy sensor and was 5 mJ per pulse. The mass spectra of the clusters were averaged over 5000 laser pulses.

The extractor grids were placed on a positive bias potential of 150 V. This prevented the large majority of cations of the sizes of interest that were produced in the source from entering the acceleration stage of the TOF. This, in turn, guaranteed that the measured distribution of the fragmentation/ionization products Nb_N^+ ($N < 25$) from the multi-photon absorption did not overlap significantly with the abundance distribution of the cations created in the source.

A mass spectrum with both the extraction grid bias on and the heating/ionization laser fired is compared with a spectrum with the bias voltage off and no heating laser pulse in Fig. 2. There is little overlap of the mass abundance distributions in the two situations, and generally the intensities with heating/ionization laser pulse were higher than without.

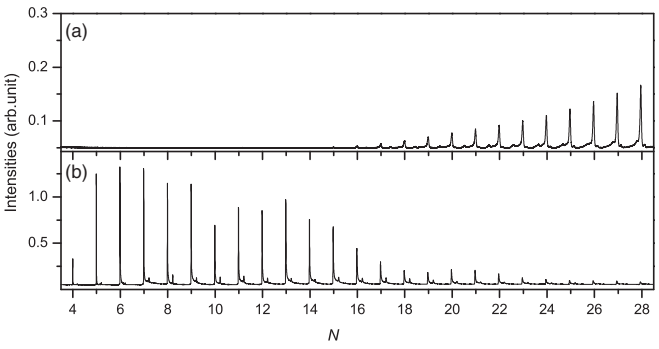

FIG. 2. Mass spectra recorded without (frame (a)) and with laser heating of the clusters in the TOF extraction region (frame (b)). Frame (a) was recorded with zero bias voltage on the acceleration grids and thus represent the cationic clusters produced in the source. In frame (b) the bias is 150 V and the signal originated from neutral clusters that were ionized and fragmented by the heating laser pulse. In frame (b), the extraction of the ions was delayed by 1 μs after the heating laser pulse.

After ionization, cationic clusters were extracted into the TOF by a pulsed high-voltage corresponding to a final kinetic energy of about 3.3 keV (for the reference potentials given in Fig. 1) that was applied shortly after the laser pulse. Only cationic clusters reached the detector. After acceleration the clusters flew freely for 1.2 m before entering a reflectron. The field of the reflectron was slightly detuned from the optimal resolution value which had the effect that the clusters that fragmented after acceleration and before entry into the reflectron (the metastable products) appeared as peaks between parent sizes N and $N - 1$, i.e., those clusters of size N, $N - 1$ that did not undergo metastable decay in the TOF. Part of a typical spectrum is shown in Fig. 3.

The tail to larger masses on the most intense peaks in the spectrum shown in Fig. 3 is due to thermionic emission and indicates a delayed production of the ion. The determination of the thermal radiation does not require that all ionized clusters are heated beyond the evaporation limit, as is otherwise necessary for an evaporative ensemble analysis,[21] and hence the presence of this delayed tail does not cause problems for the analysis.

The metastable decay was measured in two different series of measurements. In the first, the extraction of the ions after laser excitation was delayed by 0–3.5 μs, following the procedure used in Ref. 12. The switched extraction potential had an amplitude that was independent of the switching time. All other potentials in the mass spectrometer were kept fixed. In the absence of thermal radiation, the metastable fraction in these data will give a straight line through (0, 0) when plotted vs. the quantity $\ln(t_2/t_1)$, where t_1 is the time elapsed from the excitation laser pulse to the mass selection in the TOF acceleration stage, and t_2 is the time from the laser excitation to the entry into the reflectron (see Ref. 12 or Sec. 6.6 in Ref. 21). Deviations from this zero intercept straight line indicate the presence of thermal radiation. Two typical examples of this representation of the data, for $N = 15$, 19, are shown in Fig.

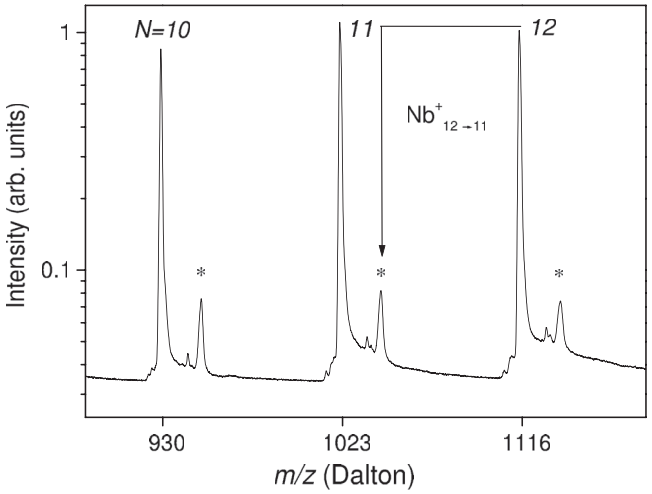

FIG. 3. A mass spectrum recorded with the Time-of-Flight mass spectrometer with a 1 μs extraction delay. Metastable products are indicated with stars. The small peaks between the parent clusters and the metastable products are Nb_NO^+ contaminations.

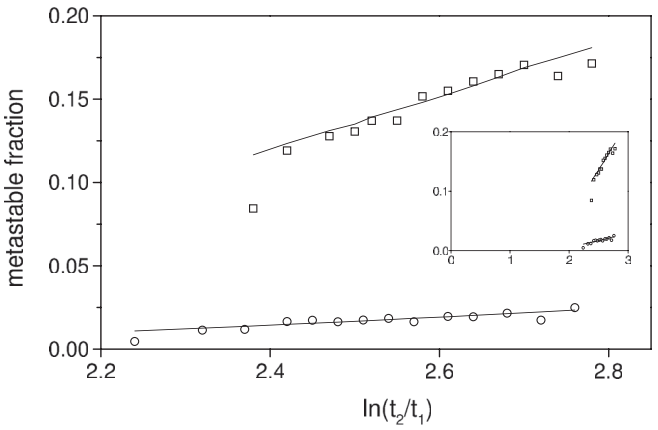

FIG. 4. The metastable decay fraction of Nb_N^+, $N = 15$ (squares) and $N = 19$ (circles) vs. $\ln(t_2/t_1)$. The curves are fits with Eq. (24), derived below. The inset shows the same data with an abscissa starting at zero. The uncertainty in the metastable fraction is mainly caused by fluctuations in the cluster production and is consistent with the average observed scatter around the fitted line.

4. These two cluster sizes are the clusters with the biggest and smallest amount of metastable decay measured. The intercept with the ordinate is clearly negative for both curves, indicating the presence of thermal radiation.

In the second set of measurements, all potentials in the mass spectrometer encountered by a cluster before the detection were scaled proportionally and the metastable decay was measured as a function of this scale parameter. In this case, the thermal radiation is manifested as a negative slope in a plot of the metastable decay vs. the reciprocal square root of the scale parameter. Equation (21) gives the dependence for weak radiation for this experimental protocol. Fig. 5 illustrates this for $N = 15$, 19. Both clearly have negative slopes, again signifying thermal radiation.

The data analysis with respect to peak integration was similar for the two procedures. The metastable product peaks are sharp and do not have a thermionic emission tail. Their area could be determined by integration and subtraction of a background defined by linear interpolation of the thermionic tails on which they are superposed. For the peaks representing clusters that do not fragment after t_1, it is not possible to separate the prompt component from the thermionic emission contribution in the TOF spectra. In order to make a consistent definition of these peak intensities, they are defined as the integral of the peak from the short time flank to a point on the delayed tail located a time $t_0 - \delta t$ after the short time flank. Here, t_0 was 3.8–4.5 μs, depending on cluster size, and δt is the extraction delay.

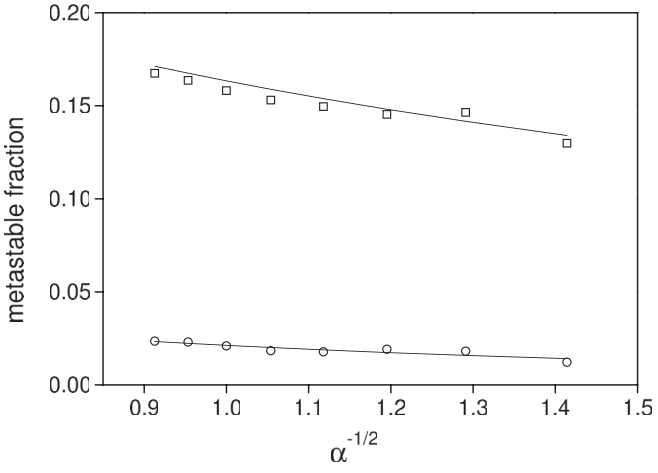

FIG. 5. The metastable decay fraction of Nb_N^+, $N = 15$ (squares) and $N = 19$ (circles) vs. $\alpha^{-1/2}$, where α is the electric field scaling parameter. The remarks on uncertainties in the caption to Fig. 4 also apply here.

For both procedures, the fitted parameters depend on the definition of t_1 and to a lesser extent of t_2. t_1 is calculated as the time it took the clusters to reach half the terminal kinetic energy, including the delay in switching the extraction voltage. Using an alternative definition of t_1 as the time it took the clusters to reach the end of the acceleration only changed the fitted values marginally. t_2 is given by the dimensions of the apparatus. The kinetic energy from the source in the co-linear configuration used was included in the calculation of both t_1 and t_2. The geometry and the timing of the ablation and excitation lasers allow a determination of the speed of the clusters to 1100 m/s. A similar value was obtained when blocking the entry electrode of the extraction region with a variable bias potential.

III. ANALYSIS

In order to extract physical parameters from the plots shown above, we will derive the relation between the parameters of the TOF, the metastable decay, and the thermal radiation. This derivation is motivated by the fact that the cooling observed here is much stronger than that observed previously for fullerenes,[12] and a critical rederivation is thus necessary.

The metastable fraction depends on the density $\rho(E, t)$ of excitation energy, E, and the rate constants. The equations that govern the time development of the density of excitation energies is

$$\frac{d\rho_N(E,t)}{dt} = -k_N(E,t)\rho_N(E,t) + k_{N+1}(E + E_{a,N+1}, t)\rho_{N+1}(E + E_{a,N+1}), \quad (1)$$

where $E_{a,i}$ is the evaporative activation energy of cluster size i, and radiation is included via the time dependence of the rate constant k.

In principle the set of equations should be solved simultaneously for all N, after initial conditions have been imposed. However, a great simplification follows from the fact that, due to the small heat capacity of the clusters, one has $k_{N+1}(E + E_{a,N+1}) \gg k_N(E)$ at all relevant energies. Similarly, all other precursors to cluster size N with energy E will have very much larger rate constants than N. This means that the term involving $N + 1$ is a product of a large factor (k_{N+1}) and an exponentially small factor which also includes k_{N+1}, and it is consequently exponentially small compared with the first term. It is therefore sufficient to retain only the first term on the right hand side of Eq. (1). For a more detailed discussion of these questions, please consult Chap. 6 of Refs. 21 or 22.

The equation is solved to (dropping the subscript N for simplicity)

$$\rho(E,t) = \rho(E,0)\exp\left(-\int_0^t k(E,t')dt'\right). \quad (2)$$

Expanding the logarithm of k to first order in t gives

$$k(E,t) = k(E,0)e^{-\mathrm{w}t}, \quad (3)$$

where

$$\mathrm{w} \equiv \frac{d\ln(k)}{dt}, \quad (4)$$

evaluated at the energy at which the rate constant is the reciprocal of the timescale, $k(E) = 1/t$. w becomes time dependent with this definition, but the time dependence is weak and w can be considered constant here. A non-zero value of w indicates the presence of thermal radiation. w has dimension of reciprocal time, and $1/\mathrm{w}$ is the crossover time from predominantly evaporative cooling to thermal radiation. A simple approximation for w will be derived below (Eq. (27)).

With constant w, the surviving population depends on E as follows:

$$\rho(E,t) = \rho(E,0)\exp\left(-\frac{k(E,0)}{\mathrm{w}}(1-e^{-\mathrm{w}t})\right). \quad (5)$$

The exponential will be essentially unity below and then drop rapidly to zero above the energy given by

$$\frac{k(E,0)}{\mathrm{w}}(1-e^{-\mathrm{w}t}) = 1. \quad (6)$$

Inverting this expression gives the cut-off energy as a function of time.

For the inversion, the most convenient procedure is to approximate the rate constant with an Arrhenius expression, $k(E) = \Omega\exp(-E_a/k_BT)$. The parameters in this expression can be extracted from experimentally determined vapor pressures. The temperature dependent vapor pressure, $p(T)$, of Nb was measured between 2000 K and 3000 K by two groups[23,24] with similar results. The data are given in the form

$$p = -A/T + B. \quad (7)$$

To find the frequency factor we have refitted these curves using the equation

$$\frac{N}{V}\overline{v}S = \Omega e^{-E_a/k_BT}, \quad (8)$$

where N/V is the vapor concentration, $\overline{v}$ is the average thermal speed, and S is the area of the gas-condensed phase interface. Using the ideal gas law for the vapor and the thermal speed $\overline{v} = (8k_BT/\pi m)^{1/2}$, where m is the mass of the atom, gives the vapor pressure

$$\frac{p}{\sqrt{k_BT}} = \left(\frac{\pi m}{8}\right)^{1/2}\frac{\Omega}{S}e^{-E_a/k_BT}. \quad (9)$$

The fit of the experimental data of Refs. 23 and 24 with this expression gives the average value

$$\Omega = S\cdot 6.2\times\ 10^{35}\mathrm{s}^{-1}\mathrm{m}^{-2}, \quad (10)$$

and $E_a = 3.37$ eV. The exact numerical value of the capture cross section is not crucial because it will appear in a logarithm of a very large number. Therefore, the cross sections can be approximated with that of a spherical particle of constant density. For cluster size N,

$$S = \pi r_1^2 N^{2/3}. \quad (11)$$

For Nb the atomic radius of $r_1 = 1.63\times10^{-10}$ m gives the frequency factors

$$\Omega = 5.1\times10^{16}N^{2/3}\mathrm{s}^{-1}. \quad (12)$$

For comparison, the same factor calculated from the detailed balance prefactor for the evaporative rate constant gives, in the first approximation (Eq. (5.11) in Ref. 21),

$$\Omega \approx \frac{m}{\pi^2\hbar^3}\pi r_1^2T^2N^{2/3}. \quad (13)$$

The value for 2500 K is $1.6\times10^{17}N^{2/3}\mathrm{s}^{-1}$. We find the agreement between the two satisfactory and will proceed with the experimental value.

Inversion of Eq. (6), where k is approximated by an Arrhenius expression, gives

$$k_BT_m(t) = \frac{E_a}{\ln\left(\frac{\Omega}{\mathrm{w}}(1-e^{-\mathrm{w}t})\right)}. \quad (14)$$

The parent temperature is then given by $T_m + E_a/2C$, where the last term is the leading order finite heat bath correction.[25,26] $T_m(t)$ is the highest temperature sustainable for the cluster at the time t after laser excitation. The absolute amount of metastable decay between the mass selection time in the primary acceleration stage, t_1, and the entry into the reflectron at t_2 is given by

$$M_{abs} = D\int_{E_m(t_2)}^{E_m(t_1)}\rho(E,t=0)dE \approx D\rho(E_m,t=0)(E_m(t_1)-E_m(t_2)), \quad (15)$$

where D is a combined transmission and detection efficiency, and E_m is the canonical energy at $T_m + E_a/2C$, i.e., the time dependent upper cutoff in the energy distribution. Approximating ρ in Eq. (15) with a constant is justified because the abundance envelope distribution is broad, indicating an equally broad initial energy distribution.[8,21]

To convert the temperatures that appear in Eq. (15) to the corresponding energies $E_m(t_i)$, the caloric curve is required. The bulk canonical caloric curve can be written as

$$\overline{E} = E_0 + C'T + \gamma T^2, \quad (16)$$

where E_0 is a constant, $C' = 3.2Nk_B$ and $\gamma = 4.1\times10^{-4}Nk_B\mathrm{K}^{-1}$.[27] Adopting this functional form for the microcanonical case (but leaving the numerical value of the coefficients as free parameters for the time being), Eq. (15) gives the amount of metastable decay,

$$M_{abs} = D\rho(E,0)\left[E_a\frac{C'}{k_B}\left(G_1^{-1}-G_2^{-1}\right)+\frac{\gamma E_a^2}{k_B^2}\left(G_1^{-2}-G_2^{-2}\right)\right], \quad (17)$$

where, for ease of notation, we have defined

$$G_i \equiv \ln\left(\frac{\Omega}{\mathrm{w}}(1-e^{-\mathrm{w}t_i})\right). \quad (18)$$

When $\mathrm{w}t_i$ is small and the heat capacity is constant, an expansion to first order in $\mathrm{w}t_i$ is meaningful and the expression for

M_{abs} reduces to

$$M_{abs} \propto \frac{1}{\ln(\Omega\bar{t})^2}\left(\ln(t_2/t_1) - \frac{1}{2}\mathrm{w}(t_2 - t_1)\right), \quad (19)$$

where $\bar{t}$ is an average time, the precise definition of which is not important. In the experiments with delayed extraction, M_{abs} is a straight line with a negative intercept which is proportional to the radiative power, as already mentioned above. In the experiments where the potentials are scaled, the times vary as $t_{i,0}/\alpha^{1/2}$, where

$$\alpha \equiv \frac{V_k}{V_{k,0}}, \quad (20)$$

and the time $t_{i,0}$ is the value for the reference set of potentials $V_{k,0}$. This gives the α dependence

$$M_N \underset{\sim}{\propto} \frac{1}{\ln(\Omega\bar{t})^2}\left(\ln(t_{2,0}/t_{1,0}) - \frac{1}{2}\mathrm{w}(t_{2,0} - t_{1,0})\alpha^{-1/2}\right). \quad (21)$$

Hence a plot of the metastable fraction vs. $\alpha^{-1/2}$ give a straight line, providing an alternative method to determine w. In the absence of radiation, the metastable fraction will show no dependence on the scaling factor of the electrical potentials. The relations in Eqs. (19) and (21) motivate the choice of axis in Figs. 4 and 5.

For larger values of w an expansion in $\mathrm{w}t_i$ becomes inconvenient because higher order terms must be included. It turns out to be a better approximation instead to expand Eq. (17) in the quantity $\ln(\frac{1-e^{-\mathrm{w}t_2}}{1-e^{-\mathrm{w}t_1}}) \equiv x$. To second order, the expansion gives

$$M_{abs} \propto \frac{E_a C'}{k_B}\frac{x}{G_1}\left(1 - \frac{x}{G_1^2}\right) + \frac{\gamma E_a^2}{k_B^2}\frac{2x}{G_1^3}\left(1 - \frac{3}{2}\frac{x}{G_1}\right). \quad (22)$$

We can evaluate the magnitude of the individual terms with the value of G_1 pertaining to acceleration times of 1μs, viz., $\ln(1\,\mu\mathrm{s}\,\Omega) \approx 28$ and use the bulk values for E_a, C', and γ. It gives

$$M_{abs} \propto 0.385Nx\,(1 - 0.036x) + 0.0049Nx\,(1 - 0.054x). \quad (23)$$

The magnitude of the higher order correction terms in Eq. (23) is such that it is reasonable to retain only the first order term in x in this expression. After division by the parent intensity, P_N, this gives the metastable fraction,

$$M_N \equiv \frac{M_{abs}}{P_N} = c\ln\left(\frac{1 - e^{-\mathrm{w}t_2}}{1 - e^{-\mathrm{w}t_1}}\right). \quad (24)$$

The parameter c depends on N. In the absence of thermionic emission and for size independent evaporative activation energies, it is of the order of $C/k_B G_1^2$,[21] where C is the heat capacity. The fits of the experimental data with Eqs. (25) and (26) gave values about twice that when $C = 4(N-2)k_B$ and $G_1 = 28$ are used. We consider this satisfactory.

For the experiments with delayed extraction, Eq. (24) can be expressed in terms of the delay δt as

$$M_N = c\ln\left(\frac{1 - e^{-\mathrm{w}(t_{2,0}+\delta t)}}{1 - e^{-\mathrm{w}(t_{1,0}+\delta t)}}\right), \quad (25)$$

where $t_{i,0}$ are the no-delay values of t_i. For simplicity, we have disregarded the source kinetic energy here. It will modify the values of Δt slightly and is taken into account in the data fitting. For the scaled potentials experiments, Eq. (24) takes the form

$$M_N = c\ln\left(\frac{1 - e^{-\mathrm{w}t_{2,0}/\alpha^{1/2}}}{1 - e^{-\mathrm{w}t_{1,0}/\alpha^{1/2}}}\right), \quad (26)$$

where α is defined in Eq. (20). The times $t_{i,0}$ are those pertaining to $\alpha = 1$, as defined above, and are chosen to be identical to the same times that appear in Eq. (25), although this is not necessary.

The results of the fits are shown in Fig. 6.

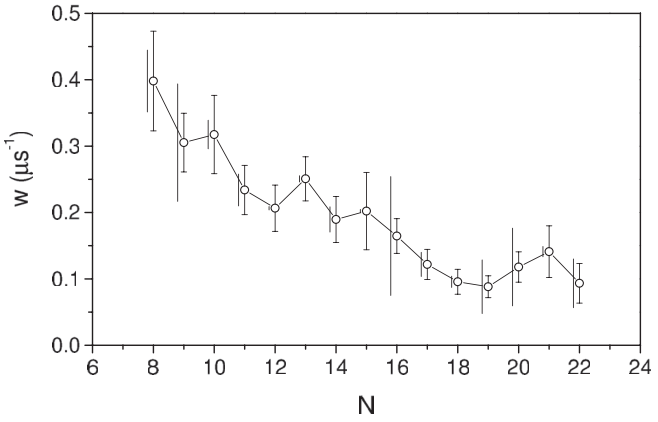

FIG. 6. The thermal radiation constant as extracted from the data with Eq. (24). The values are the average from the experiments with delayed extraction and scaled potentials. The uncertainties are the average from the fits. The full uncapped vertical lines shifted down by 0.2 span the difference between the thermal radiation constants derived using the two different approaches.

IV. DISCUSSION

From the definition of w in Eq. (4), the radiated power P can be extracted from the data. With an Arrhenius expression one has

$$\mathrm{w} = \frac{\partial \ln k}{\partial T}\frac{dT}{dE}P = \frac{E_a}{Ck_BT^2}P, \quad (27)$$

where T is the microcanonical temperature of the radiating cluster. Including the finite heat bath correction this temperature is, to next-to-leading order in $1/C$, equal to

$$k_BT = E_a\left(\frac{1}{\ln(\Omega/\mathrm{w})} + \frac{1}{2C/k_B}\right). \quad (28)$$

Inserting this into Eq. (27) gives

$$P = \mathrm{w}E_a\frac{C}{k_B}(G^{-1} + (2C/k_B)^{-1})^2, \quad (29)$$

where $G \equiv \ln(\Omega/\mathrm{w})$. The activation energy is calculated including the surface tension,

$$E_a = E_a(N) = E_a(\infty) - \frac{2}{3}BN^{-1/3}, \quad (30)$$

where B is calculated from the experimentally measured macroscopic surface tension, $\sigma = 1.94$ J/m^2,[28] to $B = 4\pi r_1^2\sigma = 4.04$ eV, and $E_a(\infty)$ is 3.37 eV, as determined

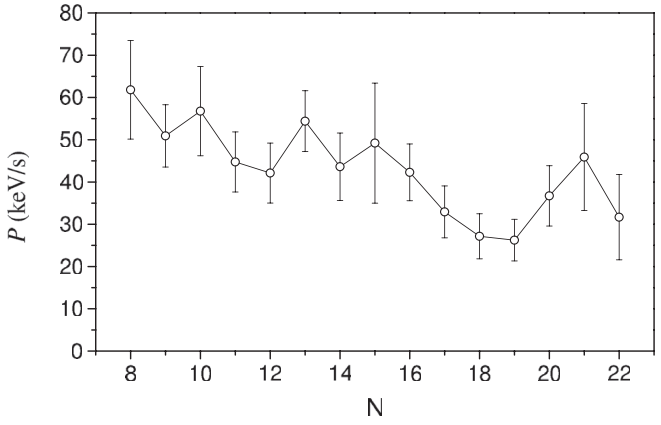

FIG. 7. The emitted power extracted from the data and Eq. (31).

by the vapor pressure data. The values for the emitted power are therefore

$$P = \mathrm{w}C/k_B \left(E_a(\infty) - \frac{2}{3} B N^{-1/3} \right) \left(\frac{1}{2C/k_B} + \frac{1}{G} \right)^2. \tag{31}$$

For C we can summarily use the values $4(N-2)k_B$. The reduction of N by two accounts for the reduction of the number of vibrational degrees of freedom for a free cluster due to the presence of rotations and translations. It is exact if the heat capacity is carried by the motion of the atoms and the electronic heat capacity can be ignored.

The emitted power is plotted as a function of cluster size in Fig. 7. As for the abundance spectra, size variations due to shell structure or odd-even effects are absent at our level of precision. Comparing with Fig. 6 we also note that the emitted power varies much less with size than w.

It is instructive to compare the radiative power with the energy lost by atomic evaporation. At the time w^{-1} where the dominant cooling mechanism crosses over from evaporation of atoms to thermal radiation, the energy loss caused by evaporation is $\mathrm{w}E_a$, which is 3–13 $\times$ 10^5 eV/s for bulk activation energies, i.e., much higher than the radiated power. This large ratio can be traced to the small heat capacity of the clusters with the following simple calculation. The ratio of power emitted in evaporation processes to the radiated power is calculated with Eq. (27) to

$$\frac{\mathrm{w}E_a}{P} = \frac{\frac{E_a}{T^2 C k_B} P E_a}{P} = \frac{G^2 k_B}{C}. \tag{32}$$

The value of G, being the logarithm of a big number, is fairly constant, about 25–30 on molecular beam time scales. For clusters with $C \lesssim k_B G^2$ the energy lost through evaporation will therefore be larger than the radiated power, even at the crossover time. For the values of the heat capacities and G used above, the critical cluster size where equality is reached corresponds to $N \approx 200$. It is noteworthy that this result is independent of the relative magnitude of the evaporative activation energy and the average energy of the emitted photons, as long as the electromagnetic radiation can be described as continuous. It predicts that for a given energy deposited into the system and a given emitted power, the photon yield increases with cluster size at the crossover region. This observation may be important for the optimization of incandescent lamps build on emission of light from nanoparticles.[10]

The weak size dependence of the emitted power shown in Fig. 7 is somewhat surprising but has parallels in other measured properties of Nb clusters. The absorption spectra of neutral Nb cluster have been measured in the visible part of the spectrum for $N = 5-15$[29] and $N = 7-20$.[30,31] Both experiments used the action spectroscopy technique with noble gas adducts, ensuring cold clusters, and both found cross sections that varied smoothly with wavelength and increased towards the blue. The shape of the cross section suggests that it is dominated by the surface plasmon resonance. The magnitude of the cross section measured in the experiments is, however, independent of cluster size. This is unexpected because a surface plasmon is a collective resonance and is expected to have an oscillator strength that grows with size. On the other hand, it is consistent with the radiated power observed here, provided the size independence of the plasmon profile extends down to typical thermal radiation photon energies.

Finally, we will briefly discuss the relevance of the data presented here for the interpretation of experiments that extract information from the amount of metastable decay. One example is experiments where dissociation energies are extracted from the amount of collision-induced decay in low energy collisions.[32] In the analysis of these experiments, the emission temperature at the end of the clusters' flight, at time t, is calculated as $E_a'/\ln(\Omega t)$, where E_a' is the putative activation energy fitted from the experiment and t is an experimental time scale which on the order of 100 μs. In the presence of radiation the decay terminates at the emission temperature $E_a/\ln(\Omega/\mathrm{w})$, however, where E_a is the true evaporative activation energy. Equating the two gives the ratio

$$\frac{E_a'}{E_a} = 1 - \frac{\ln(\mathrm{w}t)}{\ln(\Omega/\mathrm{w})}. \tag{33}$$

With the values of w between 0.1 and 0.4 $\mu\mathrm{s}^{-1}$, this gives an overestimate of the activation energy between 8% and 13% if radiation is ignored. In addition to this, also the energy transfer function in the collision needs to be revised. A more detailed analysis of the combined effects is beyond the scope of this work.

Another case where radiation is relevant is the thermionic emission laser spectroscopy reported in Ref. 16. For sufficiently intense thermal radiation, no thermionic emission will be observed. The absolute limit for detection of IR photon absorption by thermionic emission is, for pulses long compared with the radiation time, given by the condition of stationary state at the point of emission,

$$\dot{E} = \sigma I - P(T) = 0, \tag{34}$$

where $\dot{E}$ is the rate of change of excitation energy, σ is the IR photon absorption cross section, I is the light intensity, and $P(T)$ is the emitted power. With a fluence of 6 $\times$ 10^{21} cm^{-2}, a pulse length of 5 μs, a photon energy of 0.03 eV,[16] and the emitted power of 50 keV/s, the smallest photo absorption cross section that can be detected is then equal to 1.3 $\times$ 10^{-21} cm^2. Alternatively, one may use the threshold fluences of 1 to 2 $\times$ 10^{21} photons per cm^2 in Ref. 16 together with Eq. (34) to estimate the absolute photon absorption cross

sections for the four peaks measured for Nb_{13}. The cross sections become 0.4–0.8 $\times$ 10^{-20} cm^2. This estimate ignores the stimulated emission, the difference between the radiation of the cationic and neutral cluster and assumes, as mentioned, that the laser pulse is long compared with the thermal radiation time of the cluster. A detailed modeling of these effects is beyond the scope of this work.

V. SUMMARY

The unimolecular decay of laser heated niobium clusters of size $N = 8-22$ was observed to be quenched by thermal radiation on timescales ranging from 2 to 10 μs, with an approximate $1/N$ dependence. The evaporation of atoms is suppressed exponentially with time constants given by the reciprocal of these times, and the unimolecular decays therefore effectively terminate a few μs after laser excitation. The radiated power was approximately size independent and had a value of 40–50 keV/s.

ACKNOWLEDGMENTS

This work is supported by the Research Foundation - Flanders (FWO) and by the KU Leuven Research Council (BOF, GOA, and IDO programs) and the COST action MP0903 with a STSM grant to K.H.

[1]S. Maruyama, M. Y. Lee, R. E. Haufler, Y. Chai, and R. E. Smalley, Z. Phys. D **19**, 409 (1991).
[2]T. Leisner, K. Athanassenas, O. Echt, O. Kandler, D. Kreisle, and E. Recknagel, Z. Phys. D **20**, 127 (1991).
[3]A. Amrein, R. Simpson, and P. Hackett, J. Chem. Phys. **95**, 1781 (1991).
[4]E. E. B. Campbell, G. Ulmer, and I. V. Hertel, Z. Phys. D **24**, 81 (1992).
[5]G. Ganteför, W. Eberhardt, H. Weidele, D. Kreisle, and E. Recknagel, Phys. Rev. Lett. **77**, 4524 (1996).
[6]C. Walther, G. Dietrich, W. Dostal, K. Hansen, S. Krückeberg, K. Lützenkirchen, and L. Schweikhard, Phys. Rev. Lett. **83**, 3816 (1999).
[7]J. U. Andersen, E. Bonderup, and K. Hansen, J. Phys. B **35**, R1 (2002).
[8]M. Hedén, K. Hansen, F. Jonsson, E. Rönnöw, A. Gromov, E. E. B. Campbell, A. Taninaka, and H. Shinohara, J. Chem. Phys. **123**, 044310 (2005).
[9]Y. Toker, O. Aviv, M. Eritt, M. L. Rappaport, O. Heber, D. Schwalm, and D. Zajfman, Phys. Rev. A **76**, 053201 (2007).
[10]B. Weber and R. Scholl, J. Appl. Phys. **74**, 607 (1993).
[11]K. Hansen, E. E. B. Campbell, and O. Echt, Int. J. Mass Spec. **252**, 79 (2006).
[12]K. Hansen and E. E. B. Campbell, J. Chem. Phys. **104**, 5012 (1996).
[13]J. U. Andersen, C. Brink, P. Hvelplund, M. O. Larsson, B. B. Nielsen, and H. Shen, Phys. Rev. Lett. **77**, 3991 (1996).
[14]U. Frenzel, U. Kalmbach, D. Kreisle, and E. Recknagel, Surf. Rev. Lett. **03**, 505 (1996).
[15]D. A. Hales, L. Lian, and P. B. Armentrout, Int. J. Mass Spec. Ion Proc. **102**, 269 (1990).
[16]V. J. F. Lapoutre, M. Haertelt, G. Meijer, A. Fielicke, and J. M. Bakker, J. Chem. Phys. **139**, 121101 (2013).
[17]U. Frenzel, A. Roggenkamp, and D. Kreisle, Chem. Phys. Lett. **240**, 109 (1995).
[18]U. Frenzel, U. Hammer, H. Westje, and D. Kreisle, Z. Phys. D **40**, 108 (1997).
[19]B. M. Smirnov and H. Weidele, JETP Lett. **69**, 490 (1999).
[20]W. Bouwen, P. Thoen, F. Vanhoutte, S. Bouckaert, F. Despa, H. Weidele, R. Silverans, and P. Lievens, Rev. Sci. Instrum. **71**, 54 (2000).
[21]K. Hansen, *Statistical Physics of Nanoparticles in the Gas Phase* (Springer, The Netherlands, 2013).
[22]K. Hansen and U. Näher, Phys. Rev. A **60**, 1240 (1999).
[23]R. Speiser, P. Blackburn, and H. L. Johnston, J. Electrochem. Soc. **106**, 52 (1959).
[24]P. F. Woerner and G. F. Wakefield, Rev. Sci. Instrum. **33**, 1456 (1962).
[25]C. E. Klots, J. Chem. Phys. **90**, 4470 (1989).
[26]J. U. Andersen, H. Cederquist, J. S. Forster, B. A. Huber, P. Hvelplund, J. Jensen, B. Liu, B. Manil, L. Maunoury, S. Brøndsted Nielsen, U. V. Pedersen, H. T. Schmidt, S. Tomita, and H. Zettergren, Eur. Phys. J. D **25**, 139 (2003).
[27]Landolt-Börnstein, *New Series* IV/19A (Springer, 2014).
[28]P.-F. Paradis, T. Ishikawa, and S. Yoda, Int. J. Thermophys. **23**, 825 (2002).
[29]B. A. Collings, K. Athanassenas, D. M. Rayner, and P. A. Hackett, Z. Phys. D **26**, 36 (1993).
[30]W. J. C. Menezes and M. B. Knickelbein, J. Chem. Phys. **98**, 1856 (1993).
[31]M. B. Knickelbein and W. J. C. Menezes, Phys. Rev. Lett. **69**, 1046 (1992).
[32]S. K. Loh, L. Lian, and P. B. Armentrout, J. Am. Chem. Soc. **111**, 3167 (1989).